Laser drilling of AISI316L sheet: geometric feature modelling

K.Ravindra, Dr V SRIDAR PATNAIK, DR. VENKATA SARATH KUMAR GUTTLA

Assistent.prof
Department: Mechanical
Visakha Institute of Engineering & Technology,
Division,GVMC,Narava, Visakhapatham, Andhra Pradesh.

ABSTRACT

Extreme difficulty is encountered while micro-drilling AISI316L. Such an operation could benefit from the use of nonstandard machining techniques. The most effective method for micro-drilling is the use of a laser beam. Laser drilling may provide subpar results due to the beam's high heat energy and divergent convergence properties. In this study, we employ a Nd:YAG laser beam and explore how changing the laser's input parameters affects the outcomes. In order to reduce the total number of tests, we get maximum data for each trial. As a result, a rotating composite center has been included into the design. Analysing inputs and outputs using analysis of variance helps isolate influential factors. This article demonstrates that the top-hole circularity is significantly influenced by both current and gas pressure. The bottom side circularity is significantly affected by the current and the pulse frequency. The hole taper is significantly influenced by the cutting current and cutting speed.

Keywords:

ngitudinal bias correction, analysis of variance, repeated-measures design, AISI 316L, hole taper, hole circularity.

INTRODUCTION

Cutting tiny holes in cutting-edge materials is a formidable challenge. The stainless steel AISI316L is widely used in the healthcare, transportation, aviation, and aerospace sectors, among others. AISI316L is a bio-compatible material because to its exceptional material qualities, which include its high heat conductivity, good corrosion resistance, and high strength, etc. It's a key component of orthopaedics. E. Audiard et al. (2017) and A. Bharati's et al. (2013) both note its extensive usage in the biomedical and bio industrial fields. Laser drilling is employed in the medical field, the automotive industry, and many others today. In comparison to more traditional machining processes, its many advantages [A. Kekic et al., 2014] make it stand out. These advantages include the absence of tool wear, the absence of contact between the tool and the work piece, the low waste of materials, the precise hole features, and the micro-machining.

The laser beam is very powerful and uniform in color. In laser drilling, the laser beam itself serves as the cutting tool. Focusing a laser beam on a material's surface causes the laser's kinetic energy to be converted into heat, melting the substance in the process. This liquid is now being evaporated away. Using a blast of high-pressure gas, any leftover debris is expelled. Drilling a hole into the workpiece with pinpoint accuracy is the last step [I. Choudhary et al., 2012; A. Dubey et al., 2008]. Advanced materials like titanium, nickel-based alloys, AISI316L, etc. are often machined using a laser beam machining technique. High-speed steel and

AISI316L have both been machined using laser cutting. The authors observed a correlation between the cutting speed and power input and the resulting kerf width while processing steel. G. Gautam et al. (2018); K. Ghany et al. (2005); R. Goyal et al. (2016); and A. Hascalik et al. (2013) are just a few of the studies that examine the role that factors like pulse frequency (PF), power, gas pressure (GP), and cutting speed (CS) play in the formation of kerf width and heat affected zone on general metals. While some studies have shown that increasing laser power results in a wider kerf, other studies have shown that increasing cutting speed narrows the kerf. When cutting 4130 steels with a laser, PF is essential for minimizing the HAZ and KW [S. Kumar et al., 2006]. Machined HAZ from SS304 diminishes when laser power is increased. If you raise the CS, the KW will go down [A. Lamikiz et al., 2005].

DESIGN AND LAYOUT FOR PERFORMING EXPERIMENTS

The statistical approach of design of experiment known as response surface methodology (RSM) Modelling and optimization applications have benefited from this technique. In the engineering world, this technique is often used to find the best possible solution. Central composite design (CCD) is only one of the various experimental approaches used in RSM. When compared to other experimental designs, this one is by far the most effective. Typically, a second-order regression model is built for CCD [A. Pandey et al., 2013]. Equation 1 below is used to determine the ultimate number of experiments for CCD.

$$N = K^2 + 2K + C$$

.

where N = number of experiments, K = number of input parameters (4), and C= number of central run (7). The total number of experiments (N) is 31 [M Radanovich et al., 2011].

Table 1. Chemical Composition of AISI316L Sheet.

Material	Cr	Ni	Mo
% Composition	17.06%	10.17%	2.1%

In this case, a 500 W Nd:YAG laser was employed. It has a maximum output of 5 kW at a wavelength of 1064 nm. The AISI316L sheet utilized for the drilling operation was 1.8 mm thick. 150 mm x 100 mm x 1.8 mm AISI316L plate dimensions. AISI316L plate has the following physical properties: density (g/cm3) = 8.500, specific heat (J/kg0 K), melting point temperature (0 C), thermal conductivity (W/m0 K), and coefficient of thermal expansion (1 / 0 C) = 16.3, and specific heat expansion = 15.9. In Table 1 we can see the chemistry of the materials used in the study. The range of the input parameters was determined by trial-and-error tests using a 1 mm diameter hole. Table 2 lists the available input parameter levels. Unfortunately, not all potential values for the input parameters may be considered in experiments. Input parameters have often been chosen based on their proximity to the nominal value [N. Rajaram et al., 2003]. All input parameters for their level in the current study are very close to their theoretical levels.

Table 2. Input parameters and their levels.

Symbol	Input Parameters (Abbreviations)	Unit	Level				
			-2	-1	0	1	2
p1	GP	{kg/cm²}	6	7	8	9	10
p2	C	{Amp}	150	175	200	225	250
p3	CS	{mm/min}	10	20	40	60	80
p4	PF	{Hz}	8	9	10	11	12

EVALUATION OF DRILLED HOLE QUALITY CHARACTERISTICS

Size of the Hole

All four sides of the hole's diameter have been measured. Its circumference has been measured at 450 intervals. The diameter of the hole was determined using a Moticam stereo microscope. Subsequently, as indicated in Figure 1 [Saini et al., 2018], we have taken the mean of the four diameters d1, d2, d3, and d4. All experiments have used the same measuring procedure. Both the top and bottom sides' hole diameters have been measured. Micrographs of the drilled hole are shown in Figure 1 and Figure 2.

Centricity and radial deviation at the hole exit; hole taper (HT)

The thermal energy of a laser beam is used to produce a hole while doing a laser drill. The edge of a laser-drilled hole isn't always exactly round. Both the bottom and top-hole radii may be calculated using equations 2 and 3. The holes you drill won't be completely round. As a result, there will be a noticeable discrepancy between the diameters on the top and bottom in any given through-hole configuration. The formula for its measurement is given in equation 4. The hole taper [Saini et al., 2018] is dependent on the sheet thickness.

$$Cent= (D_t)min \ / \ (D_t)max$$

$$Cent= (D_b)min \ / \ (D_b)max$$

$$H_T = \frac{180}{\pi}\left\{Tan^{-1}\left(\frac{D_{ent}-D_{exit}}{2t}\right)\right\}$$

where Dt= top side diameter, Db= bottom side diameter, Dent= Top side diameter, Dixit= bottom side diameter, and t= sheet thickness.
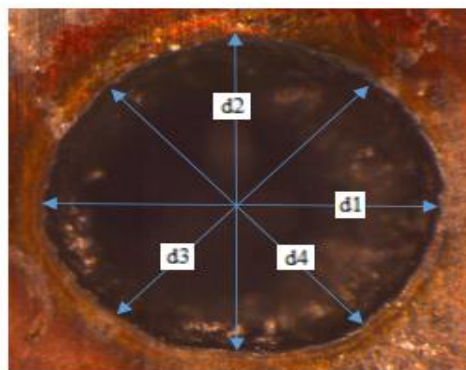

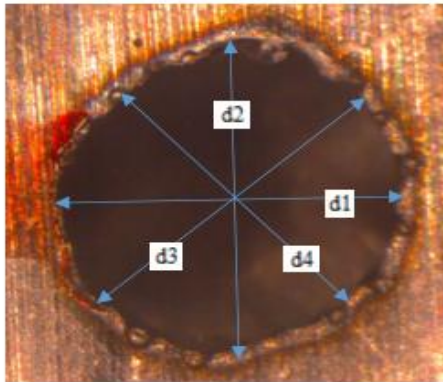Figure 1. Microscopic image of top diameter.

Figure 2. Microscopic image of bottom diameter.

REGRESSION MODEL

RSM is a mathematical tool that can be used to make a best model for multiparameter in experimental data and prepare an optimum experiment design. RSM is a trustful arithmetic technique for many applications. A mathematical relation has been prepared between input parameters and responses. This will help know the behaviour of process parameters on response. The general second-order regression equation is given in equation 5 [R. Goyal et al., 2016].

$$y_k = \alpha_0 + \sum_{i=1}^{n} \alpha_i p_i + \sum_{i=1}^{n} \alpha_i p_{ii}^2 + \sum_{i=1}^{n}\sum_{j=n+1}^{n} \alpha_{ij} p_i p_j$$

where 'α' are regression coefficients. 'n' is the number of input parameters. $yy*$ is response [S. Saini et al., 2018]. After checking acceptability of parameters, the values are given in Table 2. Second-order regression equations are developed for responses Cent, Clexit, and HT accordingly. General second-order regression equations are given in equations 6, 7, and 8 for responses Cent, Clexit, and HT, respectively, in uncoded units for AISI316L as follows:

$Cent = -1.672 + 0.2896\, p_1 + 0.00989\, p_2 + 0.00384\, p_3 + 0.0632\, p_4 - 0.01210\, p_1^2 - 0.000015\, p_2^2 - 0.000030\, p_3^2 - 0.00053\, p_4^2 - 0.000332\, p_1{}^*p_2 + 0.000131\, p_1{}^*p_3 - 0.00302\, p_1{}^*p_4 - 0.000007\, p_2{}^*p_3 - 0.000071\, p_2{}^*p_4$

$- 0.000071\, p_3{}^*p_4$

$Cexit = 1.10 - 0.071\, p_1 + 0.01075\, p_2 - 0.00797\, p_3 - 0.190\, p_4 + 0.00093\, p_1^2 - 0.000025\, p_2^2 - 0.000002\, p_3^2 + 0.00343\, p_4^2 - 0.000579\, p_1{}^*\, p_2 + 0.001247\, p_1{}^*p_3 + 0.01369\, p_1{}^*p_4 + 0.000057\, p_2{}^*p_3 + 0.000298\, p_2{}^*p_4$

$- 0.001473\, p_3{}^*p_4$

$HT = 36.7 - 2.26\, p_1 - 0.2862\, p_2 + 0.1275\, p_3 + 1.95\, p_4 - 0.0360\, p_1^2 + 0.000458\, p_2^2 - 0.000411\, p_3^2 - 0.0330\, p_4^2$

$+ 0.01644\, p_1{}^*p_2 - 0.01654\, p_1{}^*p_3 - 0.00067\, p_3{}^*p_4$

MODEL VALIDATION

Theoretical Validation

S-value and R-value are calculated for theoretical validation of any model. These values are given in Table 3 for individual model. If correlation coefficient's value (R-value) is more than 0.9, then the predicted data will be acceptable. In the present case, R-value is more than 0.9 for each model. Now, the data given in Table 2 is well fitted for all responses [R. Goyal et al., 2016 & A. Mascali et al., 2013].

Table 3. Regression analysis of developed model.

Model Summary	S	R-sq	R-sq (adj)
Cent	0.0088	90.70%	82.57%
Cexit	0.0269	93.22%	87.29%
HT	0.2817	94.93%	90.50%

Analysis of variance (ANOVA) has been used to test the capability of models. Its results have been shown for all models in Table 4. P-values are less than 0.5 for all three models. F-ratios are also calculated for source of regressions. F-ratios are 11.21, 15.72, and 21.41 for Cent, Clexit, and HT models, respectively. F-ratios for responses are more than critical F-ratio. Confidence level is 95% [W. Tiffany et al., 1985]. So, the developed experimental relations for all parameters are significant. It also acceptable for prediction of responses value.

Table 4. ANOVA result for Responses.

Source	DF	F-Value			P-Value		
		Cent	Cexit	Cent	Cexit	Cent	Cexit
Regression	14	11.15	15.72	11.15	15.72	11.15	15.72
Linear	4	15.56	3.22	15.56	3.22	15.56	3.22
Square	4	27.13	2.62	27.13	2.62	27.13	2.62
2-Way Interaction	6	2.92	12.51	2.92	12.51	2.92	12.51
Error	16						
Lack-of-Fit	9	1.63	2.98	1.63	2.98	1.63	2.98
Pure Error	7						
Total	30						

Important ANOVA Factor Analysis

important input parameters for the answers have been identified using this method. Table 5 displays

the obtained outcomes. Cent relies heavily on gas pressure and current. Clexit is particularly sensitive to both the current and the pulse frequency. For HT, both the cutting current and the cutting speed are crucial.

Table 5. P-values of input parameters for responses.

Process Parameters	Cent	Cexit	HT
Gas Pressure	0	0.601	0.125
Current	0	0.041	0
Cutting Speed	0.085	0.231	0.035
Pulse Frequency	0.18	0.032	0.195

Experimental Validation

Table 6. Mean prediction error for different responses.

Exp. No.	Input parameters				Cent			Cexit			HT		
	p1	p2	p3	p4	Pred.	Expe.	% error	Pred.	Expe.	% error	pred.	Exp.	% error
1	7	175	20	11	0.93	0.92	1.29	0.90	0.93	3.49	7.95	7.57	5.01
2	9	175	20	11	0.95	0.94	0.69	0.93	0.91	2.61	7.05	6.81	3.54
3	7	225	20	11	0.96	0.95	1.48	0.95	0.95	0.35	5.27	5.32	1.03
4	9	225	20	11	0.95	0.93	1.67	0.93	0.96	2.96	6.01	5.84	2.92
5	7	175	60	11	0.95	0.93	1.71	0.67	0.65	3.44	8.47	8.53	0.73
6	9	175	60	11	0.97	0.96	1.14	0.81	0.84	3.77	6.25	5.85	6.76
7	7	225	60	11	0.96	0.94	2.57	0.84	0.86	2.08	6.26	5.92	5.78
8	9	225	60	11	0.96	0.94	1.70	0.92	0.92	0.02	5.68	5.73	0.89
9	7	175	60	11	0.95	0.93	1.71	0.67	0.67	0.36	8.47	8.61	1.70
10	9	175	20	9	0.92	0.91	1.46	0.88	0.90	1.70	7.00	6.90	1.48
11	7	225	20	9	0.94	0.91	2.85	0.93	0.93	0.08	5.80	5.75	0.86
12	9	225	20	9	0.93	0.92	1.03	0.85	0.90	5.25	6.60	6.35	3.98
13	7	175	60	9	0.92	0.89	2.39	0.80	0.80	0.50	8.41	8.14	3.37
14	9	175	60	9	0.95	0.94	1.44	0.88	0.89	1.44	6.25	6.20	0.81
15	7	225	60	9	0.94	0.92	2.36	0.94	0.97	3.51	6.84	7.09	3.47
16	9	225	60	9	0.95	0.92	2.79	0.96	0.96	0.08	6.33	6.26	1.04
17	6	200	40	10	0.92	0.91	0.88	0.87	0.91	4.71	7.26	7.16	1.44
18	10	200	40	10	0.94	0.91	2.92	0.93	0.94	1.43	5.84	6.10	4.13
19	8	150	40	10	0.93	0.92	0.65	0.76	0.78	2.34	9.15	9.41	2.81
20	8	250	40	10	0.95	0.92	3.31	0.90	0.94	4.30	6.54	6.42	1.83
21	8	200	10	10	0.94	0.91	3.01	0.94	0.94	0.44	6.24	6.61	5.63
22	8	200	80	10	0.94	0.93	1.38	0.83	0.88	5.61	6.16	6.12	0.65
23	8	200	40	12	0.99	0.97	2.45	0.88	0.93	4.89	6.30	6.51	3.29
24	8	200	40	8	0.95	0.94	1.15	0.93	0.94	1.14	6.84	6.77	0.96
25	8	200	40	10	0.98	0.95	2.71	0.89	0.90	0.76	6.70	6.62	1.17
26	8	200	40	10	0.98	0.96	1.64	0.89	0.93	3.96	6.70	6.41	4.49
27	8	200	40	10	0.98	0.96	1.64	0.89	0.89	0.36	6.70	6.80	1.51
28	8	200	40	10	0.98	0.95	2.71	0.89	0.93	3.96	6.70	6.66	0.56
29	8	200	40	10	0.98	0.97	0.59	0.89	0.90	0.76	6.70	6.91	3.07
30	8	200	40	10	0.98	0.97	0.59	0.89	0.89	0.36	6.70	6.49	3.20
31	8	200	40	10	0.98	0.96	1.64	0.89	0.93	3.96	6.70	6.47	3.52

Experimental validation: experimental data will be compared with the predicted regression model. Mean prediction percentage error (MPPE) will be found out for all the responses.

MPPE value is calculated by the formula given in equation 9:

$$MPPE = \frac{(\text{Experimental value} - \text{Predicted value})}{(\text{Experimental value})} * 100$$

Table 6 displays the comparison's results along with the prediction error for each answer type. As you can see in Table 6, each answer has a projected value, an experimental value, and a percentage error. Results for MPPE are 1.8% for the Cent answer, 2.2% for the Clexit response, and 2.8% for the HT response. Every one of these numbers is within the range of acceptability. All of the models that have been created are obviously valid and satisfactory. These may now be utilized as forecasting models [B. Yilbas, 1996; B. Yilbas, 2008].

AN ANALYSIS BASED ON PARAMETERS

The Top-Level Improvement of Circularity (Cent)

Due to the thermal energy of the laser beam, hole circularity has always been a significant reaction in hole characteristics. Table 5 shows how the gas pressure and current have a role in determining the hole's entry circularity (Cent). Figure 3: A Regression Plot
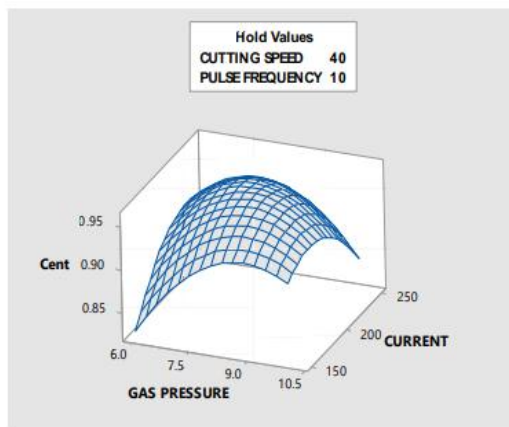
Figure 3. Cost per square centimeter, gas pressure, and amperage as a function of plotted surface area.

Figure 3 shows that when gas pressure and current are increased, Cent initially rises until they reach their midpoint. From then on forth, Cent drops as gas pressure and current get up. At 8 kg/cm2 gas pressure and 200 A current, the maximum Cent is 0.97 (experimental value). When the current is over 200A, the laser power is sufficient to melt the metal on the top surface of the work piece, and when the gas pressure is above 8 kg/cm2, the molten metal is removed from the surface as quickly as possible. As a result, the material will quickly melt or burn, and the melting temperature surrounding the hole's periphery will rise. Rapid waste removal is possible because to the high gas pressure. Because of this, the molten material will take off a larger amount, which will result in a less spherical peak.

Strengthening the Base's Circularity (Clexit)

An increase in bottom-side hole circularity may be achieved by adjusting the pulse frequency and current. Figure 4 presents a visualization of the response surface for this. The behaviour is well seen in this reaction surface plot.

Clexit's current equals Cent's. Until around the middle of the current's range, raising it enhances circularity. After that, however, it decreases. Exit circularity likewise rises in tandem with the pulse frequency up to its maximum value. At 200 A and 9 Hz pulse frequency, the highest value of Clexit observed in experiments was 0.96. The laser beam's repetition rate grows as the pulse frequency increases. As a result, the laser beam will penetrate more targets. When the current is raised at the same time, undesired substances may be melted and scraped off surfaces more rapidly. The resulting holes will be more round.
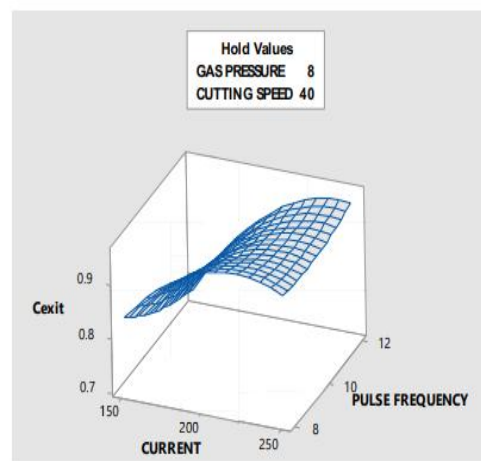

Figure 4. Map of the surface A comparison of Clexit, Pulse Frequency, and Current.

Hole Taper Improvement (HT)

Significant factors for hole taper are current and CS. During the process of creating a hole, the laser beam's converging and diverging characteristics cause the hole to be tapered. A homogeneous hole diameter (from top to bottom) is achieved by setting HT to its bare minimum, which also enhances the hole's other characteristics. Prior sections of this document have already covered its most important aspects. Figure 5 depicts a plot of a response surface for this. Hole taper is decreasing with increasing current, as seen in Figure 5. An increase in cutting speed will cause the hole taper to grow. Reduced hole taper is achieved by increasing the current to its maximum value while maintaining a slow cutting speed. With 200 A of current and 20 mm of cutting per minute, a hole with a taper of 5.320 may be made. Since AISI316L is a very thermally conductive material, the molten substance may be quickly evacuated despite the high current value. When cutting speed and gas pressure are both low (Table 6), molten surface material cannot be scraped away, and the residual solids recast and stick to the hole's perimeter. As a result, there will be less of a gap between the two holes' diameters.
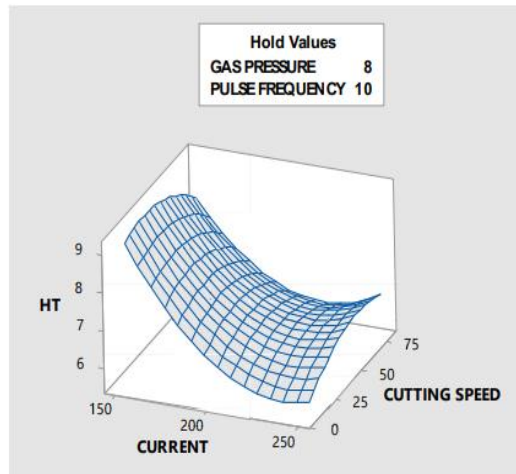
Figure 5. Graph of the Surface Cutting Velocity vs. HT vs. Current.

CONCLUSION

Experimental modelling of laser drilling of AISI316L sheet for 1 mm hole diameter has been prepared using THE Design of experiment. Validation of all responses and input parameters has been performed using RSM and ANOVA methods. The following are the results from this study. It's permissible and reliable to use a regression model for all replies (Cent, Clexit, and HT). All of the t-test p-values are lower than 0.05. b. The average proportion of wrong predictions for Cent, Clexit, and HT answers are 1.8%, 2.2%, and 2.8%, respectively. Top-side circularity is shown to be largely dependent on current and gas pressure (Cent). At 8 kg/cm2 of gas pressure and 200 A of current, the maximum Cent value is 0.97 (experimental value). Bottom-side circularity is shown to be significantly affected by current and pulse frequency (Clexit). At 200 A and 9 Hz pulse frequency, the highest value of Clexit observed in experiments was 0.96. d) Hole taper is significantly influenced by the current and cutting speed. With a cutting speed of 20 mm/min and a minimum current of 200 A, the hole taper may be set to 5.320.

REFERENCES

[1]Audiard E, Lopez J, Ancelot B, Gaudian K, Kling R, Motty E 2017. Optimization of surface engraving quality with ultrafast laser. Journal of Laser Applications. 29 (2).

[2]Bharati's A, Murthy HN, Anand B, Madhusudan CD, Praveen GS, Krishna M. 2013. Characterization of hole circularity and heat affected zone in pulsed CO2 laser drilling of alumina ceramics. Optics and Laser Technology. 53: 22–32.

[3] Kekic A, Begic-Hajdarevic D, Kaurenoic M, Omerspahic A. 2014. CO2 laser cutting of alloy steels using N2 assist gas, Procedia Engineering. 69: 310–315.

[4] Choudhury IA, Chong WC, Vahid G. 2012. Hole qualities in laser trepanning of polymeric materials. Optics and Lasers Engineering. 50 (9): 1297–1305.

[5] Dubey AK, Yadava V. 2008. Laser beam machining—a review. International Journal of Machine Tools and Manufacture. 48 (6). 609–628.

[6] Gautam GD, Pandey AK. 2018. Pulsed Nd:YAG laser beam drilling: A review. Optics and Laser Technology. 100: 183–215.

[7] Ghany KA, Newishly M. 2005. Cutting of 1.2 mm thick austenitic stainless-steel sheet using pulsed and CW Nd:YAG laser. Journal of Mtls Processing Technology. 168 (3): 438–447.

[8] Goyal R, Dubey AK. 2016. Modelling and optimization of geometrical characteristics in laser trepan drilling of titanium alloy. Journal of Mechanical Science and Technology. 30: 1281–1293.

[9]Mascali A, Ay M. 2013. CO2 laser cut quality of Inconel 718 nickel – based superalloy. Optics and Laser Technology. 48: 554–564.

[10] Lamidi A, Lasalle D, Sa JA, Lo LN. 2005. CO2 laser cutting of advanced high strength steels (AHSS). Applied Surface Science. 242: 362–368.

[11Montgomery DC. 2015. Design and analysis of experiments. Wiley. Pandey AK, Dubey AK. 2013. Fuzzy expert system for prediction of kerf qualities in pulsed laser cutting of titanium alloy sheet, Machining Science and Technology. 17 (4): 545–574.

[12] Radanovich MMM. 2011. Experimental investigations of CO2 laser cut quality: A review. Nonconventional Technologies.4. Rajaram N, Sheikh-Ahmad J, Cheraghi S. 2003.

[13]CO2 laser cut quality of 4130 steel. International Journal of Machine Tools and Manufacture. 43 (4): 351–358.

[14] Saini SK, Dubey AK, Upadhyay BN, Choubey A. 2018. Study of hole characteristics in Laser Trepan Drilling of ZTA. Optics and Laser Technology. 103: 330 –339.

[15] Tiffany WB. 1985. Drilling, Marking and Other Applications for Industrial Nd:YAG Lasers. SPIE, Application of High-powered Laser. 527: 28–36. Yilbas BS. 1996.

[16]Experimental investigation into laser cutting parameters. Journal of materials processing technology. 58: 323–330. Yilbas BS. 2008.

[17] Laser cutting of thick sheet metals: effects of cutting parameters on kerf size variations. Journal of materials processing technology. 201: 285–290.